ADVANCED MATERIALS
www.advmat.de

Lessons from the Ocean: Whale Baleen Fracture Resistance

Bin Wang, Tarah N. Sullivan, Andrei Pissarenko, Alireza Zaheri, Horacio D. Espinosa, and Marc A. Meyers**

Whale baleen is a keratin-based biological material; it provides life-long (40–100 years) filter-feeding for baleen whales in place of teeth. This study reveals new aspects of the contribution of the baleen's hierarchical structure to its fracture toughness and connects it to the unique performance requirements, which require anisotropy of fracture resistance. Baleen plates are subjected to competing external effects of hydration and varying loading rates and demonstrate a high fracture toughness in transverse loading, which is the most important direction in the filtering function; in the longitudinal direction, the toughness is much lower since delamination and controlled flexure are expected and desirable. The compressive strength is also established and results support the fracture toughness measurements: it is also highly anisotropic, and exhibits a ductile-to-brittle transition with increasing strain rate in the dry condition, which is absent in the hydrated condition, conferring impact resistance to the baleen. Using 3D-printing prototypes that replicate the three principal structural features of the baleen plate (hollow medulla, mineralized tubules, and sandwich-tubular structure) are created, and the role of its structure in determining its mechanical behavior is demonstrated. These findings suggest new bioinspired engineering materials.

Baleen is the filter-feeding apparatus inside the oral cavity of mysticetes (baleen whales) and allows for efficient feeding on great quantities of small zooplankton; this filtering mechanism has enabled the mysticetes to evolve into the largest living creatures on earth. The teeth are replaced by baleen, which separates prey from water. It therefore has to withstand a wide variety of forces from both water flow and prey. The fracture toughness, which measures the structural integrity for reliable functioning, is a crucial material property[1] for baleen.

Dr. B. Wang
Shenzhen Institutes of Advanced Technology
Chinese Academy of Sciences
Shenzhen 518055, China
E-mail: bin.wang@siat.ac.cn
Dr. T. N. Sullivan, A. Pissarenko, Prof. M. A. Meyers
University of California
San Diego, La Jolla, CA 92093, USA
E-mail: mameyers@eng.ucsd.edu
A. Zaheri
Theoretical and Applied Mechanics Program
Northwestern University
Evanston, IL 60208, USA
Prof. H. D. Espinosa
Department of Mechanical Engineering
Northwestern University
Evanston, IL 60208, USA

DOI: 10.1002/adma.201804574

Although baleen is basically a keratinous material, it is uniquely different from the keratin in terrestrial (such as bird feathers, pangolin scales, mammal horns, and hooves) and other marine animals (e. g., turtles). Whale baleen is the most mineralized of the keratins;[2] it consists of a series of parallel plates suspended from the palate down both sides of the mouth.[3] These plates are frayed on their inner edge into bristles (**Figure 1**a,b). Baleen is known to be both strong and flexible; it was a popular material used in corsets from the 11th to the 20th centuries, and has been used in basketry in Alaskan Native art. The bristles resemble hair fibers[4] and are responsible for forming a fine net,[5] while the plates, with a tubular structure,[6] sustain life-long hydrodynamic forces and withstand collisions from copepods, euphausiids, and fish.[3,7]

Here, we identify and quantify the principal mechanisms of toughening in whale baleen, and correlate these to structural design aspects. We also establish the effects of hydration and loading rate. Baleen-inspired prototypes are 3D printed to identify key aspects of the structure in compression. We provide below a number of efforts focused on applying the lessons learned from nature. Wegst et al.[1] review the most obvious design characteristics of a number of natural structural materials, and present a roadmap for incorporating them into bioinspired designs. Nacre-inspired composite films that are highly stretchable have been produced.[8] The use of bidirectional freeze casting to generate bioinspired structures was discussed by Bai et al.[9] Chen et al.[10] introduced a methodology for metal ion synergetic crosslinking in polymers to increase significantly mechanical properties. Additive manufacturing has been used to reproduce the tridimensional structure of conch shell and enabled the identification of design criteria for impact resistance.[11] Tridimensional manufacturing has facilitated the generation of architected structures with composite beams providing both increased strength and toughness, a characteristic of biological materials.[12] In a similar manner, insights about the structural design of baleen for tailored fracture resistance can serve to stimulate further research with the ultimate goal of developing new advanced materials for novel applications.

The baleen plates of bowhead whales have a distinct sandwich-tubular structure (Figure 1b,c): a solid shell enclosing a porous (tubular) layer, with the central tubule region varying from ≈26% to nearly 100% of the plate's thickness toward the

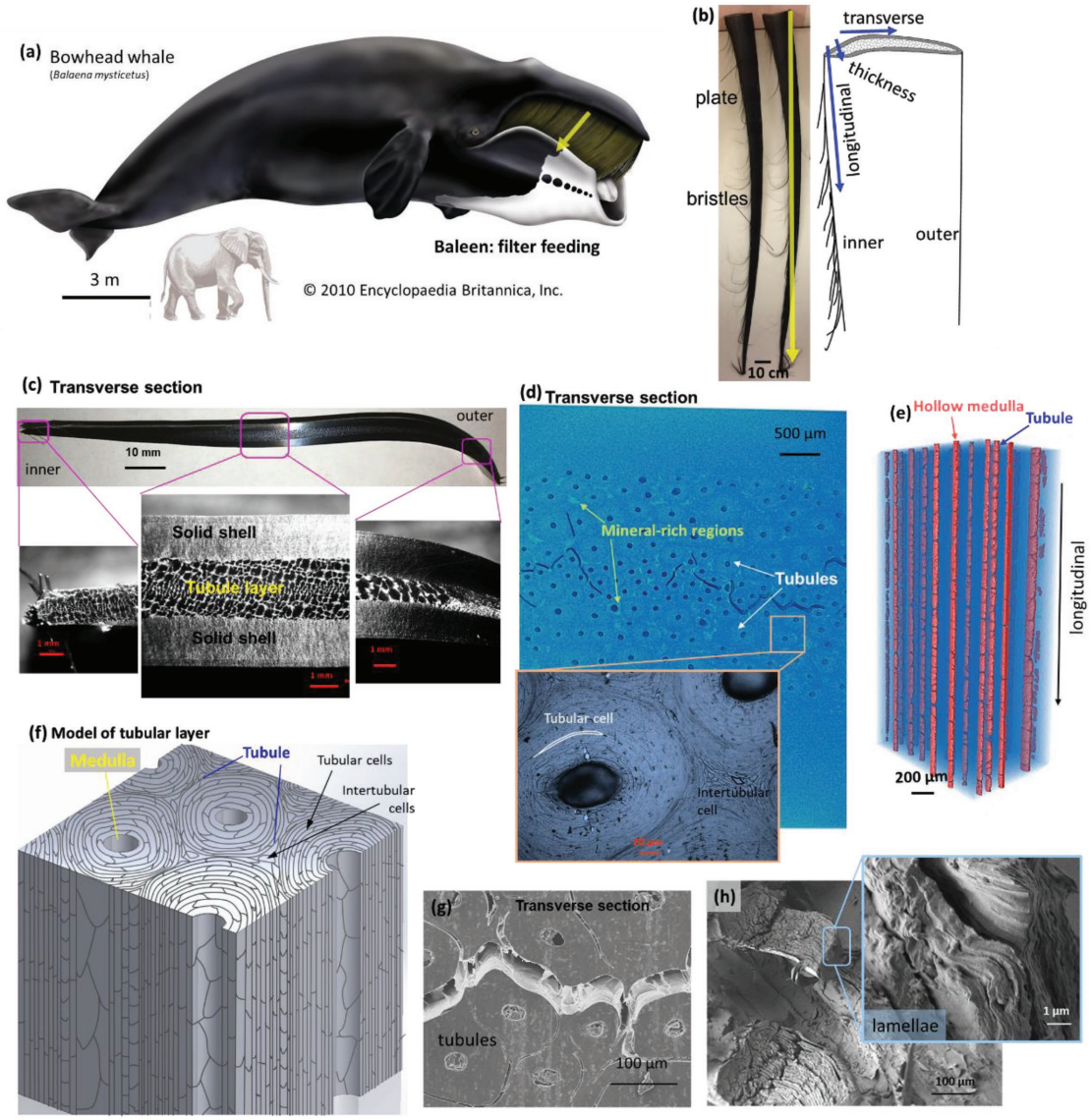

Figure 1. Bowhead whale and its baleen. a) Bowhead whale; the yellow arrow indicates the direction from which the baleen hangs. Bowhead whale image adapted with permission. Copyright 2010, Encyclopedia Britannica, Inc. b) Two baleen plates, and the longitudinal, transverse, and thickness directions. c) Transverse sections of the baleen plate. d) 3D reconstructions from micro-CT transverse section, with an inserted optical microscopy image showing the tubular and intertubular cells, and e) the hollow medullae aligned in longitudinal orientation. f) A structural model of the tubular layer showing the tubular and intertubular cells. g) SEM of transverse section of tubular layer, and h) transversely fractured surface showing the tubular lamellae.

inner end. The inner end consists of bristles, each one formed by a separate tubule. X-ray microcomputed tomography of a rectangular section reveals the three regions and the mineral-rich locations within intertubular material (yellow arrows in Figure 1d). A much higher calcium content is found in the tubular layer than in the solid shell (2.7 times in dry weight) (Section SI, Supporting Information). The random distribution of minerals (crystalline hydroxyapatite) is confirmed by elemental mapping through scanning electron microscopy (SEM) (Section SII, Supporting Information). This agrees with the X-ray diffraction of bowhead baleen revealing a random array of hydroxyapatite crystals.[13] The hollow cores of the tubules (Figure 1e) indicate their longitudinal orientation.

The central layer is mostly composed of tubules cemented by intertubular material (≈3% volume fraction of the entire layer, except for the inner end, Figure 1). A structural model of this layer is shown in Figure 1f: all tubules are formed by flattened keratinized cells (about 1–3 µm thick) arranged in concentric layered lamellae around a central hollow medulla, while intertubular cells are squeezed between tubules (Figure 1d–h). Tubules have a characteristic diameter varying from 60 to 900 µm (including the medulla) (Figure 1d,g,h). The intertubular cells are not as flattened and have a height-to-width ratio of ≈1.[6] They also form lamellae between tubules. The tubular lamellae and the solid shell of the plate consist of longitudinally aligned microscale fibers (Figure S2, Supporting Information),

which is confirmed from measurements of the elastic moduli in the longitudinal (average 270 MPa) and in the transverse (average 200 MPa) tubule sections, obtained by nanoindentation (Section SIII, Supporting Information). As an α-keratinous material, baleen[2,6,14] consists of intermediate filaments (≈7 nm diameter) embedded in an amorphous matrix,[14] which form macrofibrils (100–400 nm) and further organize into microscale fibers. Nanoscale intermediate filaments with hydroxyapatite crystals form the mineralized regions.

This hierarchical structure of baleen plates is distinct from tubular structures seen in other biological materials. The macroscale sandwich-tubular structure of baleen has mineral-rich regions (Figure 1c,d), while horns and hooves solely have a tubular structure without minerals,[15] and the sucker rings of squid exhibit ordered proteinaceous nanoscale tubules.[16] The baleen's sandwich-tubular structure resembles other natural solid shell-over-cellular core structures, which generate high flexural stiffness-to-weight and strength-to-weight ratios.[17] However, compared to other keratinous sandwich structures (e.g., the feather rachis), baleen is stiffer due to its higher hydroxyapatite content, since the incorporation of minerals into a biopolymer boosts its stiffness and yield strength.[18] These tubules can deform and shear between each other when a baleen plate is bent, the plate deforming like a thin beam.

The critical energy required to propagate a preexisting crack can be determined through the *J*-integral, a measure of the toughness incorporating both elastic and plastic deformation, often under static loading. For precracks oriented in the transverse direction, the *J*–*R* curves (**Figure 2**a) show an increase of *J* with growing crack length Δa: the *J*-integral for dry baleen reaches a peak value of ≈18 kJ m^{-2} (higher than other keratinous materials, e.g., 5.5–10.7 kJ m^{-2} for hoof wall[15]) over a very small amount of crack extension, indicating an excellent resistance to crack propagation and fracture. This is due to the structural toughening mechanisms, which can be classified into intrinsic and extrinsic.[18,19] In addition to intrinsic toughening (demonstrated in the stress-whitening in the inelastic zone around the crack tip, similarly observed in nacre,[20] bone,[18,19] and semicrystalline polymers[21]), baleen undergoes extrinsic toughening due to fiber bridging and significant crack deflection (Figure 2a,b,e). The cracks growing in the transverse direction are arrested and redirected along the tubules, enhancing resistance to fracture and increasing *J*; once a crack enters a tubule, it is deflected along the weak interface between tubular lamellae rather than penetrating through them (Figure 2e). The solid shell also contributes to crack deflection. Hydrated baleen demonstrates lower but still increasing *J*-integral values, with similar toughening mechanisms present (Figure 2a).

For cracks growing in the longitudinal orientation, ambient dry baleen plates exhibit initially rising *R*-curves but reaching a much lower *J*-integral toughness (2.0–2.5 kJ m^{-2}); hydrated plates generate comparable *J*-integral values as ambient dry experiments. The crack front exhibits a white zone and moderate fiber bridging (Figure 2c,d). Failure propagates longitudinally since the direction of maximum driving force is parallel to the path of the "weakest" microstructure resistance (Figure 2f). The whitening at the crack front due to inelastic deformation of polymer chains in both orientations allows the material to dissipate energy while sustaining force.

The anisotropy in fracture behavior of baleen plates is a necessity because transverse fracture would cause breakage of the baleen and failure to perform its filtering function, whereas splitting longitudinally into bristles refines the filter, if it occurs in a controlled manner.

Hydration has been widely known to soften keratinous materials through water–matrix protein interactions (increases the interchain space and breaks down secondary bonding, thus increasing chain mobility).[14,22] Cracks propagating in the longitudinal direction demonstrate a more significant decrease in flexural modulus from ambient dry to hydrated conditions than those traveling transversely; this is due to the anisotropic fibrous nature, whether the load is sustained mostly by the water-sensitive matrix or by the water-insensitive fibers (Figure S5, Supporting Information). As the *J*-integral value is inversely related to the modulus (Section SIV, Supporting Information), this leads to the different changes of *J* from ambient dry to hydrated conditions between longitudinal and transverse loadings (Section SV, Supporting Information). In longitudinal loading, hydration does not significantly affect toughness. In transverse loading, despite the decrease in toughness (*J*-integral) from dry to hydrated conditions, extrinsic toughening mechanisms effectively restrict crack propagation and the toughness values are higher than those in longitudinal loading.

In support of the toughness measurements, quasistatic and dynamic compression results (Section SVI, Supporting Information) confirm the anisotropy of strength. The strain-rate sensitivity is characteristic of keratinous materials, as the comparison in **Figure 3**a indicates. The strain-rate sensitivity of the hydrated samples was much higher ($m \approx 0.09$–0.11) than the dry specimens ($m \approx 0.02$–0.03); this significant difference is attributed to an increased viscosity of the hydrated specimens, enabled by the water molecules penetrating into the amorphous matrix and plasticizing it. The elastic modulus and strength are significantly higher in the parallel than in the perpendicular direction (Figure 3b). The Voigt and Reuss averages, which, respectively, apply to the parallel and perpendicular directions, explain these differences.

$$E_{\text{Voigt}} = V_{\text{ha}} E_{\text{ha}} + V_{\text{k}} E_{\text{k}} \tag{1}$$

$$\frac{1}{E_{\text{Reuss}}} = \frac{V_{\text{ha}}}{E_{\text{ha}}} + \frac{V_{\text{k}}}{E_{\text{k}}} \tag{2}$$

The indices ha and k designate the two principal components, hydroxyapatite and keratin. Note that $V_{\text{ha}} + V_{\text{k}} \leq 1$ due to the presence of voids. These equations predict a higher elastic modulus in the parallel than in the perpendicular direction. The averaged strengths follow the same relationship. This is maintained in the hydrated condition.

Microstructurally, the plates show tubule and fiber buckling and separation at 10^{-3} s^{-1}, and fragmentation with dynamic loading. This embrittlement at higher strain rates is a manifestation of a ductile-to-brittle transition, which has been observed previously for keratin in the toucan beak.[24] Fracture toughness tests were also conducted at higher loading rates (Section SVII, Supporting Information), demonstrating that the fracture

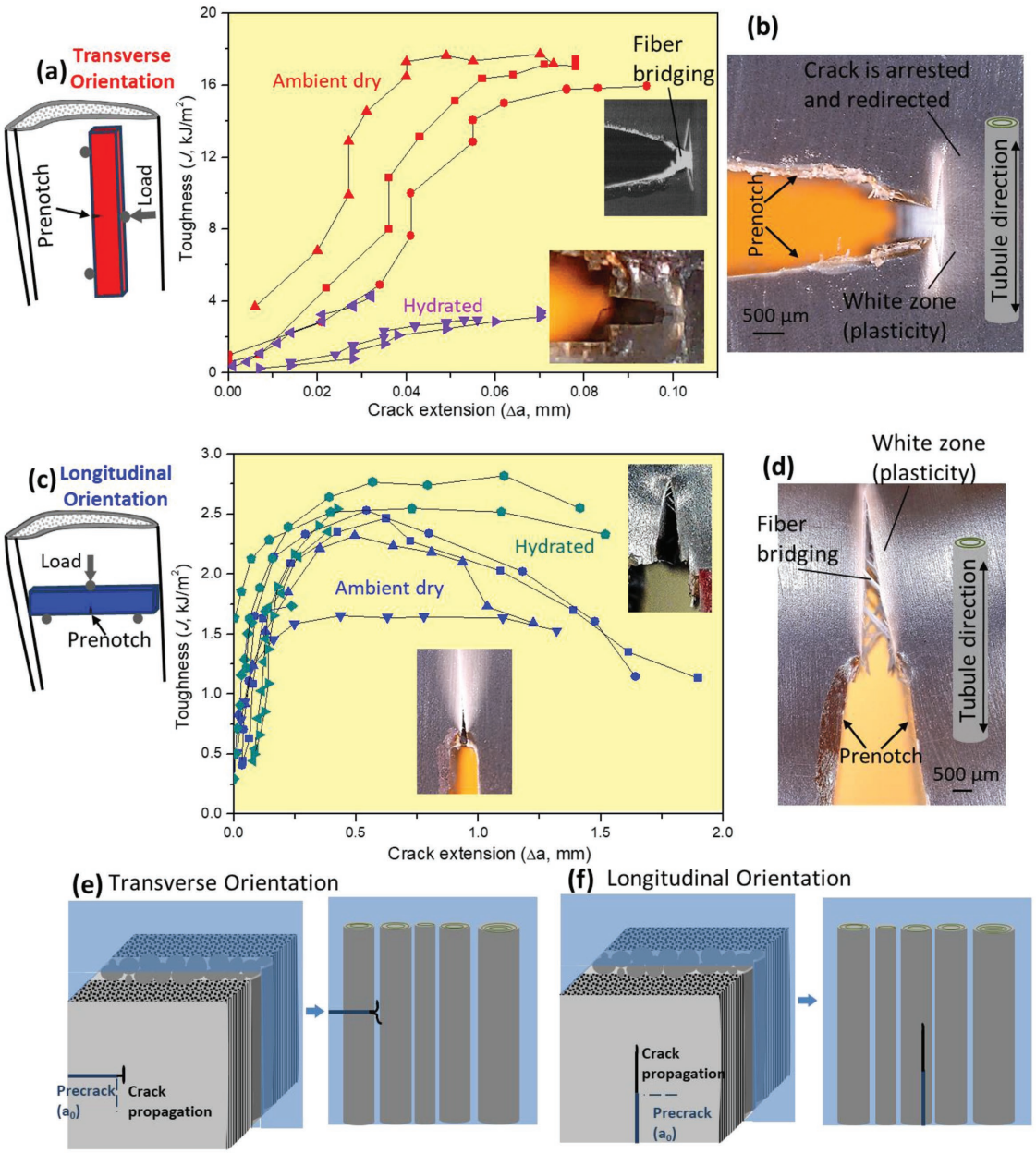

Figure 2. Fracture behavior of baleen plates. a) Toughness (*J*)–crack-resistance (*R*) curves of baleen plates loaded in transverse orientation in ambient dry and hydrated conditions, with each curve representing one sample in 12 periodic load–unload tests. b) Optical microscopy image at the crack tip region from (a) after 12 load–unload cycles. c) Toughness (*J*)–crack-resistance (*R*) curves of baleen plates loaded in longitudinal orientation in both conditions, with each curve representing one sample in 12 periodic load–unload tests. d) Optical microscopy image at the crack tip region from (c). e,f) Fracture behavior in the transverse (e) and longitudinal (f) orientations.

toughness (*J*) decreases with increasing loading rate; this is a direct consequence of the ductile-to-brittle transition.

Aside from this, hydration leads to larger deformability before failure: baleen plates in dynamic compression loading show cracks and shearing along the tubule boundaries, due to these mineral-rich regions, and the solid shell exhibits delamination rather than fragmentation. Up to a strain of −0.35 no failure is observed in compressive loading at 10^3 s^{-1} of the hydrated specimen; indeed, the stress at this strain is equal to the one in quasistatic loading (Figure S6c, Supporting Information). This effect is even more pronounced for the perpendicular direction (Figure S6d, Supporting Information). In contrast, in the dynamic compression tests on the dry specimens (Figure S6a,b, Supporting Information) the dynamic stresses drop close to zero at this strain, indicating significant strain rate governed embrittlement. As mentioned earlier, hydration enhances deformability via interactions between water molecules and the keratin proteins, while dynamic loading reduces material resilience and stiffens the structure due to increased resistance to shearing. However, the increased

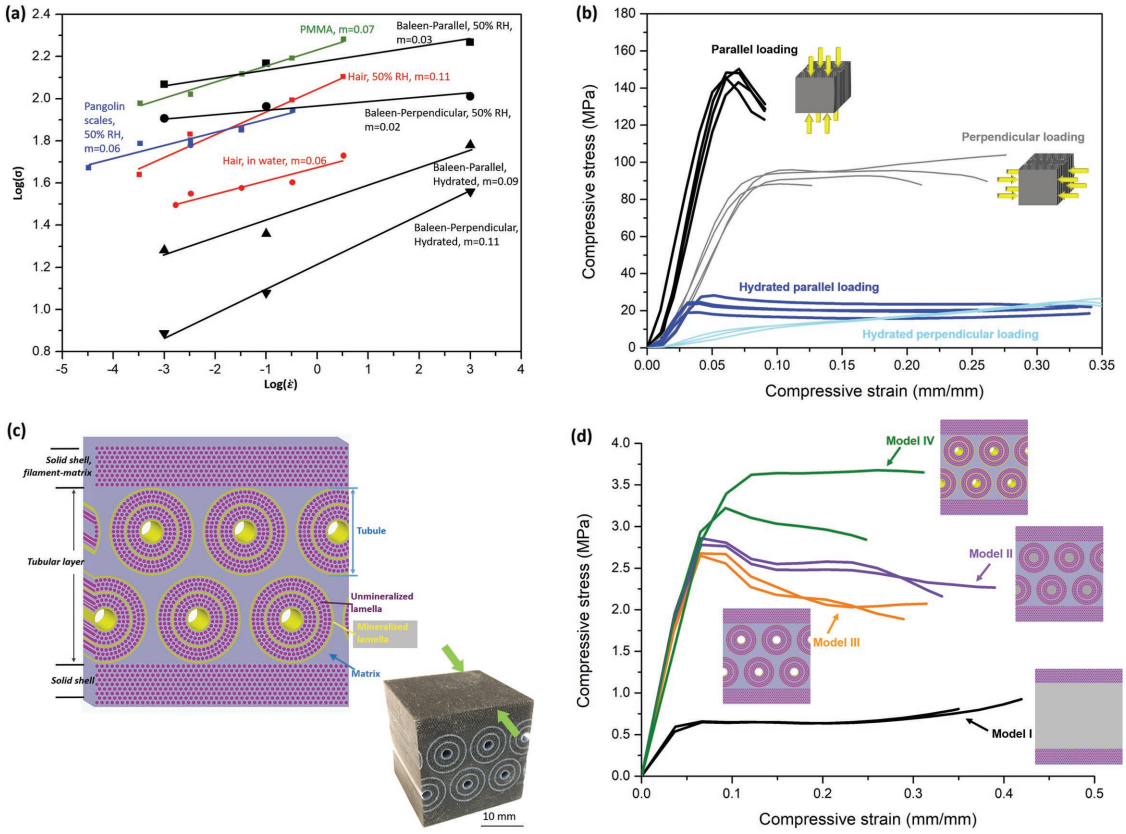

Figure 3. Quasistatic and dynamic compressive response of baleen plate and bioinspired 3D-printed samples. a) Strain-rate sensitivities (slope of log stress σ vs log strain rate $d\varepsilon/dt$) of hydrated and ambient dry baleen compared with other keratinous materials and PMMA. Adapted with permission.[23] Copyright 2016, Elsevier B.V. b) Compressive stress–strain curves of hydrated and ambient dry baleen plates in parallel and perpendicular loading directions tested at a rate of 10^{-1} s^{-1}; note the considerable anisotropy. c) Structural model of the baleen plate; inset shows the printed model where green arrows indicate the loading direction for (d). d) Structural models I, II, III, and IV with corresponding compressive behavior at a loading rate of 0.28 s^{-1}.

stiffness is not necessarily accompanied by embrittlement, which is the case for the hydrated specimens. Together, these two competing factors suggest an overall enhanced toughness and impact resistance (see Figure S6, Supporting Information), resilience prevailing over strain-rate stiffening for the hydrated condition.

Structural models were created and 3D printed (Figure 3c), highlighting the main features of baleen, including a sandwich-tubular structure, a filament-matrix shell, and tubules composed of mineralized lamellae separated by relatively unmineralized filament-matrix layers[2,25] (Section SVIII, Supporting Information). In the models, filaments have a diameter of 400 µm and mineral rings are 200 µm thick. The mineralized lamellae were modeled with a stiff polymer, the matrix with a soft polymer, and the filaments with a polymer of intermediate stiffness (details in Section SIX, Supporting Information). The printed models show similar compressive and fracture toughness properties as those of natural baleen (Figure S10, Supporting Information). Several structural models (I, II, III, and IV) were 3D printed, each model adding a structural feature to the previous one to further elucidate the role of structure in the compressive response of baleen as a function of loading rate (Figure 3d and Section SX, Supporting Information). All four models show clear stiffening and strengthening with increasing loading rate (details in Section SX, Supporting Information). The introduction of the tubules (Model II), which consist of concentric layers of filaments embedded in a matrix, significantly increases the compressive strength, as the soft material is replaced by an intermediate stiff material mimicking the filaments. Hollow cores were found to cause a slight increase in strength (Model III) at 10^{-2} s^{-1} and small decreases at 10^{-4} and 0.28 s^{-1} (Section X, Supporting Information); incorporation of the stiff "mineral" component (Model IV) leads to a clear increase in rate stiffening and strengthening. These models provide information on the evolutionary optimization of the baleen's structural design. Baleen plates require sufficient stiffness and strength to sustain external forces, yet must be lightweight to function efficiently. For these reasons, synergy of a solid shell, tubules with hollow cores, and mineralized lamellae as reflected in Model IV provide the best mechanical performance, as shown in Figure 3d.

In conclusion, baleen provides reliable filter feeding through anisotropic fracture toughness and hierarchical features which allow for efficient compressive strength. The current work provides new insights on how structure plays a role with competing factors of hydration and loading rate in fracture. It is also demonstrated, by using advanced multimaterial 3D-printed models and analysis, that the structure plays a key role in the

mechanical performance: the incorporation of hollow tubules composed of filament-matrix lamellae and mineralization, and a solid shell provides the best response. These findings serve to stimulate further studies in baleen for the ultimate goal of creating engineered advanced materials.

Experimental Section

Materials: Intact natural baleen plates (Figure 1b) from bowhead whales (*Balaena mysticetus*) were purchased from an Alaskan provider, a member of the Barrow whaling community, who are authorized to hunt whales under the Marine Mammal Protection Act and International Whaling Commission. The baleen plates had been cleaned and polished and were kept frozen with no other treatment prior to study. This research was conducted under a Federal Fish and Wildlife Permit.

Structural Characterization: Baleen segments were cut and polished for observation in an Axio fluorescence microscope and a Zeiss Sigma 500 scanning electron microscope and were further coated for observation in a Phillips XL30 scanning electron microscope. X-ray microcomputed tomography (MicroXCT-200, Xradia, CA) was used for imaging baleen segments (≈5 × 5 × 4 mm) with a 2.5 µm voxel size. The images and 3D reconstructed models were developed using the Amira software.

Fracture Toughness: Single-edge notched bend specimens were tested in Mode I loading following the ASTM 1280 guideline (Figure S4, Supporting Information) by periodic load–unload–reload experiments. An Instron 3367 testing machine with crosshead speeds of 0.05 and 0.5 mm s^{-1} was used, with specimens in two orientations (loading and precrack parallel to the longitudinal direction and loading and precrack perpendicular to the longitudinal direction (transverse orientation)) and in both ambient dry and hydrated conditions (immersed in deionized water for 4 d) tested. Specimens have final depth (W) ≈10 mm, thickness (B) ≈5 mm, and support length (S) ≈40 mm. Additional details are provided in Section SIV (Supporting Information).

Quasistatic and Dynamic Compression: Cubic specimens (≈5 × 5 × 5 mm) with loading parallel to the longitudinal direction (Para-Ori) and loading perpendicular to the longitudinal direction (Perp-Ori) (Figure S4,f, Supporting Information) and in both ambient dry and hydrated conditions were tested. All specimens were cut from the baleen plate and polished. For strain rates of 10^{-3} and 10^{-1} s^{-1}, an Instron 3367 machine was used. For impact compression (10^{3} s^{-1}), specimens were tested in a split-Hopkinson (Kolsky) bar.

Baleen Prototypes: A series of structural model of baleen were created using a computer-aided 3D interactive application and SolidWorks and were fabricated using a Stratasys Objet350 Connex3 3D printer, which can print multiple polymers with different mechanical properties simultaneously, at a high resolution (≈85 µm accuracy). The printed baleen prototypes and the models were tested in compression (30 × 30 × 30 mm) at different strain rates (10^{-4}, 10^{-2}, and 0.28 s^{-1}) using an Instron 3367 testing machine.

Supporting Information

Supporting Information is available from the Wiley Online Library or from the author.

Acknowledgements

J.-Y.J. assisted in micro-CT. The authors thank Prof. Michael Tolley and Frances Su, Tom Kalisky, and Benjamin Shih for help in 3D printing, Prof. Olivia Graeve and Kyungah Seo for TGA experiments, Eric Bushong for micro-CT scan, Ryan Anderson for SEM, and Michael Chon for discussions. This research was supported by the National Natural Science Foundation of China (51703240), a Multi-University Research Initiative through the Air Force Office of Scientific Research (AFOSR-FA9550-15-1-0009), and the Shenzhen Peacock Program (110811003586331).

Conflict of Interest

The authors declare no conflict of interest.

Keywords

baleen, fracture toughness, impact resistance, keratin, sandwich-tubular structure, whale

Received: July 16, 2018
Revised: September 4, 2018
Published online: November 19, 2018

[1] U. G. K. Wegst, H. Bai, E. Saiz, A. P. Tomsia, R. O. Ritchie, *Nat. Mater.* **2015**, *14*, 23.
[2] L. J. Szewciw, D. G. de Kerckhove, G. W. Grime, D. S. Fudge, *Proc. R. Soc. B: Biol. Sci.* **2010**, *277*, 2597.
[3] A. J. Werth, *Bull. Mus. Comp. Zool.* **2001**, *156*, 189.
[4] C. J. Pfeiffer, *Aquat. Mamm.* **1992**, *18*, 67.
[5] A. Pivorunas, *Sci. Rep. Whales Res. Inst.* **1976**, 37.
[6] D. S. Fudge, L. J. Szewciw, A. N. Schwalb, *Aquat. Mamm.* **2009**, *35*, 226.
[7] A. Pivorunas, *Am. Sci.* **1979**, *67*, 432.
[8] N. Zhao, M. Yang, Q. Zhao, W. Gao, T. Xie, H. Bai, *ACS Nano* **2017**, *11*, 4777.
[9] H. Bai, Y. Chen, B. Delattre, A. P. Tomsia, R. O. Ritchie, *Sci. Adv.* **2015**, *1*, e1500849.
[10] K. Chen, J. Ding, S. Zhang, X. Tang, Y. Yue, L. Guo, *ACS Nano* **2017**, *11*, 2835.
[11] G. X. Gu, M. Takaffoli, M. J. Buehler, *Adv. Mater.* **2017**, *29*, 1.
[12] J. Mueller, J. R. Raney, K. Shea, J. A. Lewis, *Adv. Mater.* **2018**, *30*, 1705001.
[13] D. J. St. Aubin, R. H. Stinson, J. R. Geraci, *Can. J. Zool.* **1984**, *62*, 193.
[14] B. Wang, W. Yang, J. McKittrick, M. A. Meyers, *Prog. Mater. Sci.* **2016**, *76*, 229.
[15] M. A. Kasapi, J. M. Gosline, *J. Exp. Biol.* **1997**, *200*, 1639.
[16] A. Miserez, J. C. Weaver, P. B. Pedersen, T. Schneeberk, R. T. Hanlon, D. Kisailus, H. Birkedal, *Adv. Mater.* **2009**, *21*, 401.
[17] L. Gibson, M. Ashby, *Cellular Solids: Structure and Properties*, Cambridge University Press, Cambridge, UK **1997**.
[18] M. E. Launey, P. Y. Chen, J. McKittrick, R. O. Ritchie, *Acta Biomater.* **2010**, *6*, 1505.
[19] R. O. Ritchie, *Nat. Mater.* **2011**, *10*, 817.
[20] F. Barthelat, H. D. Espinosa, *Exp. Mech.* **2007**, *47*, 311.
[21] A. Pawlak, A. Galeski, A. Rozanski, *Prog. Polym. Sci.* **2014**, *39*, 921.
[22] B. Wang, W. Yang, V. R. Sherman, M. A. Meyers, *Acta Biomater.* **2016**, *41*, 60.
[23] Y. Yu, W. Yang, B. Wang, M. A. Meyers, *Mater. Sci. Eng., C* **2017**, *73*, 152.
[24] Y. Seki, M. S. Schneider, M. A. Meyers, *Acta Mater.* **2005**, *53*, 5281.
[25] F. G. E. Pautard, *Nature* **1963**, *199*, 531.

